The validation of polarimetric rainfall estimates using R(Z,Z_{DR}) and R(Z,Z_{DR},K_{DP},A_H) in Korea

C.-H. You[1], M.-Y. Kang[2] and D.-I. Lee[1,2]

[1]{Atmospheric Environmental Research Institute, Pukyong National University, Busan, South Korea}

[2]{Department of Environmental Atmospheric Sciences, Pukyong National University, Busan, South Korea}

Correspondence to: D.-I. Lee (leedi@pknu.ac.kr)

Abstract

To improve the accuracy of polarimetric rainfall relations for heavy rainfall, an extreme rainfall case was analysed and some methods were examined. The observed differential reflectivity (Z_{DR}) quality check was theoretically investigated using the relation between the standard deviation of differential reflectivity and cross correlation, and the light rain method for Z_{DR} bias was also applied to the rainfall estimation. The best performance for this heavy rainfall case was obtained when the moving average of Z_{DR} over a window size of 9 gates was applied to the rainfall estimation using horizontal reflectivity (Z_H) and Z_{DR} and to the calculation of Z_H bias. The differential reflectivity calculated by disdrometer data may be an alternative to the vertical pointing scan for calculating Z_{DR} bias. Comparing the statistical scores between The most accurate R(Z,Z_{DR}) and R(Z,Z_{DR},K_{DP},A_H) in this study, R(Z,Z_{DR}) had better performance than that of R(Z,Z_{DR},K_{DP},A_H). However, R(Z,Z_{DR},K_{DP},A_H) is expected to be less sensitive especially to Z_H and Z_{DR} errors in both observations and simulations. Therefore, R(Z,Z_{DR},K_{DP},A_H) could be used as a representative rainfall relation in case Z_{DR} bias was not calculated accurately in Korea.

1 Introduction

Weather radar is a very useful remote sensing instrument for estimating rainfall amount due to its high spatial and temporal resolution compared with other instruments. Calculations of radar

rainfall are based on the relationship between reflectivity (Z) and rain rate (R) known as the Z–R relation (hereafter $R(Z)$). Experimentally measured drop size distributions (DSDs) have been extensively used to obtain both radar reflectivity and rain rate (Compos and Zawadzki, 2000). It can be shown that there is no unique global R(Z) relation because DSDs can vary from storm to storm and even within the storm itself (You et al., 2010). There have been a few studies on the calculation of the R(Z) relationship using disdrometer data with rainfall types and rain gage adjusted rainfall amount for operational Doppler weather radars in Korea (Jang et al., 2004; You et al., 2004; Suk et al., 2005).

Radar rainfall estimation may be contaminated by uncertainties such as hardware calibration, partial beam filling, rain attenuation, bright band, and non-weather echoes (Wilson and Brandes, 1979; Austin, 1989). To mitigate these problems, particle identification algorithms have been developed using polarimetric parameters for improving data quality control and rainfall estimates by discriminating non-meteorological artefacts such as anomalous propagation, birds, insects, second trip echo, and melting layer detection (Ryzhkov and Zrnic, 1998; Vivekanandan et al., 1999; Giangrande et al., 2008). The improvement of radar rainfall accuracy is a major reason for using polarimetric radar (Ryzhkov and Zrnic, 1996; May et al., 1999; Bringi and Chandrasekar, 2001). Ryzhkov et al. (2005a) developed a rainfall algorithm using polarimetric radar for the prototype WSR-88D (Weather Surveillance Radar-88 Doppler) system using different drop shape assumptions. Ciffelli et al. (2011) compared two rainfall algorithms, CSU-HIDRO (Colorado State University-Hydrometeor IDentification of Rainfall) and JPOLE (Joint Polarization Experiment)-like, in the high plains environment. Ryzhkov et al. (2014) recently investigated the potential use of specific attenuation (A_H) for rainfall estimation with X-band and S-band radar and found that the $R(A_H)$ method yields robust estimates of rain rates even at S band where attenuation is very small.

As a result of these theoretical and other experimental studies, many countries are replacing or modifying their radars and using polarimetric radar operationally. There are three major agencies that operate radars to monitor and forecast severe weather and flash flooding operationally in Korea: the Ministry of National Defense (MND), the Ministry of Land, Infrastructure and Transportation (MoLIT), and the Korea Meteorological Administration (KMA), with the MoLIT the first to install polarimetric radars in Korea. The KMA installed an S-band polarimetric radar in the far northwest of Korea in 2014. For successful operational implementation of these radars, considerable research on rainfall estimation, hydrometeor

classification, and DSD retrieval is required. However, there have been few studies on these polarimetric related issues other than the derivation of relationships using long period disdrometer data and the assessment of each relation after applying a very simple quality control for differential phase shift (You et al., 2014). You et al. (2014) found that the accuracy of rainfall estimation using horizontal reflectivity (Z_H) and differential reflectivity (Z_{DR}) obtained by DSDs in the Busan area in Korea was better than that obtained with relations calculated by DSDs measured in Oklahoma in the US. A quality control algorithm and unfolding of differential phase shift (Φ_{DP}) for calculating specific differential phase (K_{DP}) were applied to the rainfall estimation (You et al., 2014). Recently, You et al. (2015a) proposed a relation combining many polarimetric variables of the form $R(Z,Z_{DR},K_{DP},A_H)$ as a candidate for an optimum rainfall relation for S-band polarimetric data in Korea; this would allow a single relation to be used for different hydrometeor regimes in the absence of a stable hydrometeor classification algorithm. However, there are still issues to be resolved in improving Z_{DR} data quality and the robustness of $R(Z,Z_{DR},K_{DP},A_H)$ for the heavy rainfall case where error propagation from each polarimetric variable can occur.

This paper discusses how to improve the accuracy of rainfall estimation using moving averaged differential reflectivity and examines the robustness of the $R(Z,Z_{DR},K_{DP},A_H)$ relation for a heavy rainfall case in Korea. Sect. 2 describes the rain gage, DSD and radar dataset, together with the calculation of polarimetric variables from DSDs and the validation methods. Sect. 3 provides Z_H and Z_{DR} bias correction, an examination of Z_{DR} data quality, and the statistical results of rainfall estimation using observed and moving-average Z_{DR}. Sect. 4 contains a discussion of a possible method for improving $R(Z,Z_{DR})$ accuracy and the robustness of the $R(Z,Z_{DR},K_{DP},A_H)$ relation. Finally, we provide some conclusions in Sect. 5.

2 Data and methodology

2.1 Gage, disdrometer and radar dataset

The rainfall data from rain gages operated by the KMA were used to evaluate the accuracy of radar rainfall. Rain gages located within the radar coverage area at distances from 5 to 95 km of the radar are included in the analysis. Fig. 1 shows the location of all instruments used in this study. The circle is the radar coverage, the solid rectangle is the centre of the Bislsan radar, the plus signs show the rain gages within the radar coverage and the open rectangle is the location of a PARSIVEL (PARticle Size VELocity) and POSS (Precipitation Occurrence Sensor System;

detailed specifications are provided by Sheppard, 1990) disdrometer installed ~82 km away from the radar.

Relations for converting radar variables into rain rate are required because the radar does not observe rainfall directly. To calculate these relations, disdrometer data that can measure the DSDs are needed. One-min DSDs obtained by the POSS from 2001 to 2004 were used. To improve the accuracy of Z_{DR}, DSDs observed by PARSIVEL on 23 August 2012, 8 September 2012 and 25 August 2014 were used because POSS data were not available at that time. The PARSIVEL disdrometer is a laser-optic system that measures 32 channels from 0.062 to 24.5 mm (detailed specifications are given by Loffler-Mang and Joss, 2000).

Unreliable data, defined as belonging to the following categories, were removed: 1-min rain rate less than 0.1 mm h^{-1}; total number concentrations of all channels less than 10; drop numbers counted only in the lower 10 channels (0.84 mm for POSS and 1.187 mm for PARSIVEL); and drop numbers counted only in the lower 5 channels (0.54 mm for POSS and 0.562 mm for PARSIVEL) (You et al., 2015b).

Radar data were collected by the Bislsan polarimetric radar installed and operated by the MoLIT in Korea since 2009. The transmitted peak power is 750 kW, beam width is 0.95°, and frequency is 2.791 GHz. The polarimetric variables are estimated with a gate size of 0.125 km. The scan strategy is composed of 6 elevation angles with 2.5-min update interval. Polarimetric variables for 0.5° elevation angle were extracted from the volume data every 10 mins for this study.

2.2 Calculation of polarimetric variables

Polarimetric variables were calculated using T-matrix scattering techniques derived by Waterman (1971) and later developed further by Mishchenko et al. (1996). The following raindrop shape assumptions are used for the calculation of variables from the DSDs:

$$\frac{b}{a} = 1.0048 + 0.500057\,D - 0.02628\,D^2 + 0.003682\,D^3 - 0.0001677\,D^4, \quad (1)$$

$$\frac{b}{a} = 1.012 - 0.01445\,D - 0.01028\,D^2, \quad (2)$$

where a, b and D are the major axis, minor axis, and equi-volume diameter of raindrop in millimetres, respectively.

Eq. (1) is for the equilibrium axis ratio derived from the numerical model of Beard and Chung (1987), which is in good agreement with the results from wind tunnel measurements. The actual shapes of raindrops in turbulent flow are expected to be different from the equilibrium shapes due to drop oscillations. Oscillating drops appear to be more spherical on average than drops with equilibrium shapes as shown by Andsager et al. (1999) in laboratory studies. They demonstrated that the shape of raindrops with diameter between 1.1 and 4.4 mm is better explained by Eq. (2). You et al. (2015a) found that combining Eq. (1) for drops less than 1.1 mm and larger than 4.4 mm with Eq. (2) for the drop diameter between 1.1 and 4.4 mm as proposed by Bringi et al. (2003) gave the best rainfall estimation compared with other drop axis ratio assumptions in Korea, and we use this combined formulation in this study. Other parameters in the T-matrix calculations include the temperature, which is assumed to be 20℃ in this study. The distribution of canting angles of raindrops is Gaussian with a mean of 0° and a standard deviation of 7°, as determined recently by Huang et al. (2008).

AH was calculated from the radial profile of the attenuated reflectivity and two-way PIA (Path Integrated Attenuation) along the propagation path using observed ZH, differential phase shift from BSL radar. The more detailed description for AH calculation can be found in You et al. (2015a).

2.3 Validation

The three rainfall events occurred on 23 August 2012, 8 September 2012, and 25 August 2014, which were caused by indirect effect of Typhoon, low pressure accompanied with the front, and low pressure, respectively, were used to validate the rainfall relations. Fig. 2 shows the time series of hourly rainfall and accumulated rainfall from the three gages, ID 945 (Daebyung site), ID 255 (North Changwon site), and ID 926 (Jinbook site) that recorded the highest rainfall within the radar coverage area at each day. The daily accumulated rainfall values were around 210 mm, 150 mm, and 269 mm for these gages. The time period analysed for each event was from 0900 LT to 1700 LT (Case 1), from 0100 LT to 0600 LT (Case 2), and from 0900 LT to 1600 LT (Case 3), respectively (Table 1).

The normalized error (NE), fractional root mean square error (RMSE), and correlation coefficients (CC) of the rainfall relations and 121 gages were used to investigate the performance of each rainfall relation:

$$NE = \frac{\frac{1}{N}\sum_{i=1}^{N}\left|R_{R,i} - R_{G,i}\right|}{\overline{R_G}}, \quad (3)$$

$$RMSE = \left[\frac{1}{N}\sum_{i=1}^{N}(R_{R,i} - R_{G,i})^2\right]^{1/2}, \quad (4)$$

$$CC = \frac{\sum_{i=1}^{N}(R_{R,i} - \overline{R_R})(R_{G,i} - \overline{R_G})}{\left[\sum_{i=1}^{N}(R_{R,i} - \overline{R_R})^2\right]^{1/2}\left[\sum_{i=1}^{N}(R_{G,i} - \overline{R_G})^2\right]^{1/2}}, \quad (5)$$

where N is the number of radar rainfall (R_R) and gage rainfall (R_G) pairs, and $\overline{R_R}$ and $\overline{R_G}$ are the average hourly rain rates from the radar and gage, respectively. These statistical variables are calculated using hourly rainfall amounts derived from the radar and gage at the location of the gage. The radar rainfall at the rain gage was obtained by averaging rainfall over a small area (1 km × 1°) centered on each rain gage. The rainfall relations for calculating radar rainfall were obtained from the simulated polarimetric variables generated from DSDs. Fig. 3 shows the scatter plot of rain rate obtained from disdrometer and polarimetric radar rainfall relations $R(Z,Z_{DR})$ and $R(Z,Z_{DR},K_{DP},A_H)$ which are same relations used in You et al. (2015a). The CC and RMSE of $R(Z,Z_{DR})$ ($R(Z,Z_{DR},K_{DP},A_H)$) were 0.95 (0.99) and 3.5 mm h^{-1} (1.2 mm h^{-1}). The rainfall relations for validation and simulation are summarized in Table 2.

3 Results

3.1 Data quality of Z_{DR}

3.1.1 Improvement of Z_{DR} data quality using moving average

Z_{DR} is an important variable for hydrometeor classification and rainfall estimation. To check the quality of the Z_{DR} measurements, the radial profile of Z_{DR} was investigated as shown in Fig. 4. Fig. 4 (a) shows the spatial distribution of Z_{DR} at 0.5° elevation at 1401 LT on 25 August 2014. Fig. 4 (b) shows the radial profile of observed Z_{DR} (red line) and the standard deviation of Z_{DR} (black line) calculated using 9 gates along the line A–B shown in Fig. 4 (a). The average standard deviation of Z_{DR} along the line was 0.615 dB. Fig. 4 (c) shows the radial profile of the cross correlation; the average cross correlation was 0.982.

To find the accuracy of the observed Z_{DR} value, we use the theoretical relation between the standard deviation of Z_{DR} and the cross correlation following Bring and Chandrasekar (2003):

$$SD(Z_{DR}) = 10\log_{10}\left\{1+\left[\frac{2}{N}(1-|\rho_{co}|^2)\sum_{l=-(N-1)}^{N-1}(1-\frac{|l|}{N})|\rho_{co}(l)|^2\right]^{1/2}\right\}, \quad (6)$$

where SD(Z_{DR}) is standard deviation of Z_{DR}, N is the number of samples and ρ_{co} is the cross correlation, given by

$$\rho[n] = \exp(-\frac{8\pi^2\sigma_v^{\,2}n^2T_s^{\,2}}{\lambda^2}), \quad (7)$$

where ρ is the cross correlation, σ_v is Doppler width, n is sample number, and T_s is dwell time.

For a better comparison we display the correlations in *L* space, as proposed by Keat et al. (2015)

$$L = -10\log_{10}(1-\rho_{hv}), \quad (8)$$

where, ρ_{hv} is cross correlation. Fig. 5 shows the theoretical relation between the standard deviation of Z_{DR} and the cross correlation coefficient. Fig. 5 (a) shows the results obtained using the scan configuration of the Bislsan radar. The dwell time is 56 ms, number of samples is 55, and the normalised Doppler width is 0.02. Fig. 5 (a) suggests that for an accuracy of 0.1 dB in Z_{DR} with 1 ms^{-1} Doppler width, a value of L of over 3 (ρ_{hv} >0.999) is needed. Such values cannot be measured with the antenna. In Fig. 5 (b) the number of samples is 495, which corresponds to 9 gates, 1.125 km in range; an accuracy of 0.2 dB in Z_{DR} (the moving-average Z_{DR}, hereafter mZ_{DR}) is achieved with 1 ms^{-1} Doppler width and a value of L of 1.7 (ρ_{hv} >0.980).

Fig. 6 shows the results for Z_{DR} measurements at 1401 LT on 25 August 2014. Fig. 6 (a) shows the spatial distribution of a moving average Z_{DR} from 9 gates. Fig. 6 (b) shows the radial profile of the Z_{DR} (red line) and its standard deviation (black line) calculated for 9 gates along the line A–B shown in Fig. 6 (a). The average standard deviation of Z_{DR} along the ray was 0.169 dB. Fig. 6 (c) shows the radial profile of the cross correlation; the average cross correlation was 0.985. Both the standard deviation of Z_{DR} and the averaged ρ_{hv} values are very close to the theoretical values (standard deviation of Z_{DR} is 0.160 and ρ_{hv} is 0.987) as shown in Fig. 5. Therefore, in the next Sect. a 9-gage moving average Z_{DR} (i.e., mZ_{DR}) was used for absolute Z_H

bias correction and rainfall estimation, and its effect on the performance of radar rainfall estimation was examined for three events as mentioned in Sect. 2.3.

3.1.2 Absolute bias correction of Z_{DR} and Z_H

Before calculating radar rainfall, the Z_H and Z_{DR} must be corrected for system bias. Ryzhkov et al. (2005) calculated the required accuracy for classifying light rain and dry snow to be 1 dB and 0.2 dB for Z_H and Z_{DR}, respectively. The Z_{DR} bias correction is important for the absolute calibration of the radar using the self-consistency method. Gorgucci et al. (1999) proposed a vertical pointing scan of light rain to take advantage of the nearly spherical shape of the raindrops seen from below.

Ryzhkov et al. (2005b) used the elevation angle dependency of Z_{DR} as an alternative technique and concluded that the high variability of Z_{DR} in rainfall means it is not possible to achieve the required absolute calibration of 0.2 dB. They also proposed a method using the structural characteristics of the melting layer in stratiform clouds and measured the dry aggregated snow present above the melting layer, which gave a mean value of 0.2 dB at S band and an accuracy of 0.1 to 0.2 dB.

Trabal et al. (2009) evaluated two different methods using the intrinsic properties of dry aggregated snow present above the melting layer and measurements of light rain close to the ground and found that a Z_{DR} calibration accuracy of 0.2 dB or less was achieved for both events analysed when both methods are compared.

The vertical pointing data were not available for the case considered here and the scan strategy with six elevation angles does not detect the melting layer. Therefore, light rain measurements close to the ground were used to calibrate the Z_{DR} and Z_H biases using the self-consistency method in this study. Very light rain was defined by the thresholds 20 dBZ $\leq Z_H \leq$ 28 dBZ as proposed by Marks et al. (2011). The Z_H bias was determined following Ryzhkov et al. (2005b).

The Z_H biases for Case 1, Case 2, and Case 3 calculated with the self-consistency method using observed Z_{DR} and mZ_{DR} are -4.52 dB and -3.65 dB, -0.39 dB and -0.3 dB, –1.95 dB and –1.48 dB, respectively. The Z_{DR} biases for each case calculated by the very light rain method using observed Z_{DR} (0.49 dB, 0.33 dB, and 0.26 dB) and mZ_{DR} (0.39 dB, 0.33 dB, and 0.3 dB), respectively.

3.1.3 Improvement of Z_{DR} data quality using disdrometer

To improve the accuracy of rainfall estimation using $R(Z,Z_{DR})$, we examined the impact of Z_{DR} bias (as obtained from disdrometer data) on the accuracy. The DSD data were quality controlled and polarimetric variables were calculated by T-matrix simulation with the same configuration as in Sect. 2. Before applying the DSDs to rainfall estimation, 10-min rainfall amounts obtained by DSDs and gages were compared.

Fig. 7 shows the scatter plot of 10-min rainfall amount measured by PARSIVEL and the gage located less than 100 m away from PARSIVEL for three rainfall events. The daily accumulated rainfall amounts of Case 1 were 52.5 mm for the gage and 51.5 mm for PARSIVEL. The RMSE, NE, and CC between two instruments for Case 1 were 0.28 mm, 0.24, and 0.98, respectively. The daily accumulated rainfall amounts of Case 2 (Case 3) were 55.0 mm (116.0 mm) for the gage and 54.3 mm (129.4 mm) for PARSIVEL. The RMSE, NE, and CC between two instruments for Case 2 (Case 3) were 1.25 mm (0.83 mm), 0.25 (0.21), and 0.97 (0.99), respectively. For the comparison the Z_{DR} of the radar was averaged over 3 km × 3° as shown in Fig. 8. The calculated Z_{DR} biases for Case 1 were 0.16 dB for observed Z_{DR} and 0.158 dB for mZ_{DR}. The calculated Z_{DR} biases for Case 2 (Case 3) were 0.01 dB (-0.05 dB) for observed Z_{DR} and 0.007 dB (-0.07 dB) for mZ_{DR}. The Z_H biases described in Sect. 3.1.2 were used.

3.2 Validations of two rainfall relations

3.2.1 The performance of rainfall relations with different Z_H and Z_{DR} biases obtained from the observed Z_{DR} and mZ_{DR}

To investigate the performance of $R(Z,Z_{DR})$ and $R(Z,Z_{DR},K_{DP},A_H)$, which is related to the Z_H and Z_{DR} bias, NE, RMSE, and CC were calculated using hourly rainfall from each relation and from the gages. For the comparison of rainfall amount, two different Z_H and Z_{DR} biases were applied to observed variables as mentioned in Sect. 3.1. Each bias was calculated using observed Z_{DR} and mZ_{DR}.

Fig. 9 shows the scatter plot of 1 hour rainfall obtained using $R(Z,Z_{DR})$ and gage data for three cases, Fig. 9 (a) and Fig. 9 (b) for Case 1, Fig. 9 (c) and Fig. 9 (d) for Case 2, Fig. 9 (e) and Fig. 9 (f) for Case 3. In Fig. 9 (a) the Z_H bias was obtained from the observed Z_{DR} bias and the Z_{DR} biases calculated from observed Z_{DR} (blue full circles) and mZ_{DR} (red full circles). The RMSE, NE, and CC of the relation using mZ_{DR} were as much as 4.9 mm h^{-1}, 0.88, and 0.89, respectively

and the statistical scores were better than those obtained using observed Z_{DR}. In Fig. 9 (b) the Z_H bias was calculated from mZ_{DR}. The RMSE, NE, and CC of the relation using mZDR were 3.6 mm h^{-1}, 0.63, and 0.89, the performance of the relation using mZDR was better than that obtained using observed ZDR, respectively. The statistical scores using Z_H bias obtained from mZ_{DR} were higher than those of obtained from observed Z_{DR}. In Fig. 9 (c), (d), (e), and (f), the results were similar pattern to Fig. 9 (a) and Fig. 9 (b). It is considered that the accuracy of the rainfall estimate using mZ_{DR} is statistically more robust than that for the estimate based on observed Z_{DR}. The RMSE, NE, and CC for all cases to compare the performance of $R(Z,Z_{DR})$ rainfall estimates obtained using different Z_H and Z_{DR} biases are summarized in Table 3.

Fig. 10 shows the scatter plots when $R(Z,Z_{DR},K_{DP},A_H)$ is used for rainfall estimation at the same time period used in Fig. 9. Fig. 10 (a), Fig. 10 (c), and Fig. 10 (e) show the radar rainfall calculated using the Z_H bias obtained from the observed Z_{DR} bias and the Z_{DR} biases obtained from observed Z_{DR} (blue full circles) and mZ_{DR} (red full circles) for Case 1, Case 2, and Case 3, respectively. Fig. 10 (b), Fig. 10 (d), and Fig. 10 (f) show the radar rainfall obtained using Z_H bias calculated from mZ_{DR} and the Z_{DR} biases calculated form observed Z_{DR} (blue full circles) and mZ_{DR}(red full circles) for Case 1, Case 2, and Case 3, respectively. The RMSE, NE, and CC from each relation were not very different; differences of RMSE, NE, and CC in the two cases were 0.1 mm h^{-1}, 0.01, 0 for Case 1, 0.1 mm h^{-1}, 0.0, 0.0 for Case 2, and 0.2 mm h^{-1}, 0.01, and 0 for Case 3, respectively. The statistics for the comparison of radar rainfall obtained using different Z_H and Z_{DR} biases are summarized in Table 4. These results show that $R(Z,Z_{DR},K_{DP},A_H)$ is less sensitive to Z_{DR} error than $R(Z,Z_{DR})$.

3.2.2 The performance of the relations using Z_{DR} bias obtained by disdrometer

Fig. 11 shows the scatter plots of 1-hour rainfall obtained by $R(Z,Z_{DR})$ and gages for three cases. The radar rainfall was calculated after Z_{DR} bias correction using the bias result in the comparison between radar Z_{DR} and PARSIVEL Z_{DR}. The Z_{DR} biases for each case were 0.16 dB, 0.01 dB, –0.05 dB for observed Z_{DR} and 0.157 dB, 0.007 dB, –0.07 dB for mZ_{DR}. In Fig. 11 (a) the Z_H bias was obtained from the observed Z_{DR} bias and Z_{DR} biases calculated from observed Z_{DR} (blue full circle) and mZ_{DR} (red full circle) for Case 1. The radar rainfall using mZ_{DR} was better than that using observed Z_{DR} by as much as 0.4 mm h^{-1} for RMSE and 0.06 for NE. In Fig. 11 (b) the Z_H bias was calculated from mZ_{DR}; the improved rainfall estimation using mZ_{DR} is also shown. The rainfall estimation using mZ_{DR} and Z_H bias obtained by mZ_{DR}

was much better than that using observed Z_{DR} by as much as 1.3 mm h^{-1} for RMSE and 0.23 for NE. The similar patterns were obtained from Fig. 11 (e) and Fig. 11 (f). This result shows the better scores compared with the statistics shown in Fig. 7 that were obtained using Z_{DR} biases extracted from the radar Z_{DR} only. When the observed Z_{DR}, which fluctuates considerably along the ray, was applied to the rainfall estimation, the rainfall amount was much more variable with Z_H bias values than that with mZ_{DR}. According to these results, when moving average Z_{DR} (i.e., mZ_{DR}) is used with the Z_{DR} bias measured by PARSIVEL, the accuracy of rainfall estimation was improved and was more stable than that of other configurations using $R(Z,Z_{DR})$. However, these results would be changed when the drop size distribution of the rainfall system was fluctuated with height especially at the layer between radar beam and ground. And the wind effect is another limitation of this results.

Fig. 12 shows the scatter plots for $R(Z,Z_{DR},K_{DP},A_H)$ and gages for all events. The statistical scores were not very different from Z_H and Z_{DR} biases. The biggest differences of RMSE and NE for three cases between each relation were only 0.1 mm h^{-1} and 0.01, respectively. These behaviors were similar to the results obtained in Sect. 3.2.1.

3.2.3 The simulation of $R(Z,Z_{DR},K_{DP},A_H)$ using generated variables

With the relation using combined polarimetric variables, $R(Z,Z_{DR},K_{DP},A_H)$, error propagation can affect the accuracy of radar rainfall estimation because Z and KDP are usually correlated. To examine the contribution of errors from each variable, simulated polarimetric variables such as Z, Z_{DR}, K_{DP}, A_H, were generated with dimensions of 960 sizes of bins and 360 radials.

Fig. 13 shows the distribution function of the polarimetric variables generated assuming a Gaussian distribution. Fig. 13 (a) shows the occurrence frequency of Z_H generated with standard deviation of 7.0 dBZ and mean of 30.0 dBZ. Fig. 13 (b) shows the corresponding occurrence frequency of Z_{DR} with 0.5 dB standard deviation and 1.0 dB mean. Fig. 13 (c) shows the occurrence frequency of K_{DP} generated with 0.5° km^{-1} standard deviation and 1.0° km^{-1} mean. Fig. 13 (d) shows the occurrence frequency of A_H generated with 0.01° km^{-1} standard deviation and 0.0003° km^{-1} mean.

To investigate the extent of contamination of the rainfall amount by propagation of errors in each polarimetric variable for $R(Z,Z_{DR},K_{DP},A_H)$, the errors of Z, Z_{DR}, and K_{DP} ingested to simulated data were 0 to 5 dBZ with interval 0.25 dBZ, 0 to 0.6 dB with interval 0.03 dB, and 0 to 0.2 degree km^{-1} with interval 0.01 degree km^{-1}, respectively. The rain rate was calculated

by same $R(Z,Z_{DR},K_{DP},A_H)$ as applied to real data in the previous Sect.. The RMSE and NE were calculated for rainfall amount with and without error-ingested polarimetric variables. The rainfall amount obtained using the raw simulated variables was used as a reference.

Fig. 14 shows the RMSE and NE distribution of different polarimetric rainfall relations with ingested error. The magenta, black, red, green, blue, and purple lines show RMSE and NE obtained by the rainfall relations $R(Z)$, $R(K_{DP})$, $R(Z,K_{DP},A_H)$, $R(Z,Z_{DR})$, $R(K_{DP},Z_{DR})$, and $R(Z,Z_{DR},K_{DP},A_H)$, respectively. The threshold rainfall was from 0 to 300 mm h^{-1} for calculating statistical scores. Fig. 14 (a) shows the RMSE distribution of each rainfall relation with different ingested error step. The RMSE of $R(Z,K_{DP},A_H)$ is the largest of all the rainfall relations. The RMSE of $R(Z,Z_{DR},K_{DP},A_H)$ is higher than that of $R(Z)$, $R(Z,Z_{DR})$, and $R(K_{DP},Z_{DR})$ but less than that of $R(K_{DP})$. It means that not all errors from Z, Z_{DR}, and K_{DP} propagate into the $R(Z,Z_{DR},K_{DP},A_H)$. Fig. 14 (b) shows the corresponding distributions for NE. The value of NE increases in the order $R(Z,Z_{DR},K_{DP},A_H)$, $R(Z,K_{DP},A_H)$, $R(K_{DP})$, $R(K_{DP},Z_{DR})$, $R(Z,Z_{DR})$, and $R(Z)$. In Sect. 3.3 and 4.1, the statistical scores of $R(Z,Z_{DR},K_{DP},A_H)$ did not change significantly with respect to different Z_H and Z_{DR} biases. The results of the simulation and observations suggest that the accuracy of $R(Z,Z_{DR},K_{DP},A_H)$ is relatively weakly affected by errors in each polarimetric variable.

4 Conclusions

To improve polarimetric rainfall estimation and examine the candidates for an optimum rainfall relation using polarimetric variables observed from the Bislsan radar, the first polarimetric radar in Korea, the three rainfall systems were analysed.

The theoretical approach to investigate the observed Z_{DR} quality used the relation between the standard deviation of Z_{DR} and ρ_{hv} using the scan strategy parameters of the Bislsan radar. The result showed that more samples were required to achieve the theoretical accuracy in Z_{DR}. The best performance was obtained when a moving average Z_{DR} with window size of 9 gates was applied to the rainfall estimation using $R(Z,Z_{DR})$ and to the calculation of Z_H bias. The Z_{DR} quality check should be performed before using Z_{DR} for quantitative applications like rainfall estimation and hydrometeor classification for the Bislsan radar. We also expect that the light rain method for obtaining the Z_{DR} bias may be used as an alternative to the vertical pointing scan method, because the rainfall estimation using this method performed well in our case.

Using DSD data for the calculation of Z_{DR} bias might give more accurate rainfall estimation with $R(Z,Z_{DR})$, even it is limited to the homogeneous DSD at the layer between radar beam height and ground and not strong wind condition which could degrade the quality of Z_{DR} calculation form disdrometer. Comparing the statistical scores between the most accurate $R(Z,Z_{DR})$ and $R(Z,Z_{DR},K_{DP},A_H)$ in this study, $R(Z,Z_{DR})$ had better performance than that of $R(Z,Z_{DR},K_{DP},A_H)$.

However, $R(Z,Z_{DR},K_{DP},A_H)$ is expected to be less sensitive especially to Z_H and Z_{DR} errors in both observations and simulations. Therefore, $R(Z,Z_{DR},K_{DP},A_H)$ could be used as a representative rainfall relation in case Z_{DR} bias was not calculated accurately in Korea.

Acknowledgements

The authors acknowledge the Ministry of Land, Infrastructure, Transport and the Korea Meteorological Administration for providing radar data and AWS data for this work. The authors acknowledge Prof. V. N. Bringi at Colorado State University, who provided the scattering simulation code. The authors also acknowledge Prof. A. C. Illingworth at Reading University who provided valuable comments on Z_{DR} data quality. This research was funded by the Korea Meteorological Industry Promotion Agency under Grant KMIPA 2015-1050.

References

Andsager, K., Beard, K. V., and Laird, N. S.: A laboratory study of oscillations and axis ratios for large raindrops", Journal of the Atmospheric Sciences, 55, 208-226, 1999.

Austin, P. M.: Relation between measure radar reflectivity and surface rainfall, Monthly Weather Review, 115, 1053-1070, 1987.

Beard, K. V. and Chuang, C.: A new model for the equilibrium shape of raindrops, Journal of the Atmospheric Sciences, 44, 1509-1524, 1987.

Bringi, V. N. and Chandrasekar, V.: The polarimetric basis for characterizing precipitation. Polarimetric Doppler weather radar: Principles and applications, Cambridge University Press: Cambridge, UK, pp. 378-533, 2001.

Bringi, V. N., Chandrasekar, V., Hubbert, J., Gorgucci, E., Randeu, W., and Schoenhuber, M.: Raindrop size distribution in different climate regimes from disdrometer and dual-polarized radar analysis, Journal of Atmospheric Science, 60, 354-365, 2003.

Campos, E., Zawadzki, I.: "Instrumental uncertainties in Z-R relations", Journal of Applied Meteorology, 36, 1088-1102, 2000.

Cifelli, E. V., Chandrasekar, V., Lim, S., Kennedy, P. C., Wang, Y., and Rutledge, S. A.: A new dual-polarization radar rainfall algorithm: Application in Colorado precipitation events, Journal of Atmospheric and Oceanic Technology, 28, 352-364, 2011.

Giangrande, S. E. and Ryzhkov, A. V.: Estimation of rainfall based on the results of polarimetric echo classification, Journal of Climate and Applied Meteorology, 47, 2445-2462, 2008.

Gorgucci, E., Scarchilli, G., and Chandrasekar, V.: A procedure to calibrate multiparameter weather radar using properties of the rain medium. IEEE Transactions on Geoscience and Remote Sensing, 37: 269–276, 1999.

Huang, G.-J., Bringi, V. N., and Thurai, M.: Orientation angle distributions of drops after 80 m fall using a 2D-video disdrometer, Journal of Atmospheric Oceanic Technology, 25, 1717-1723, 2008.

Jang, M., Lee, D., and You, C.: Z-R relationship and DSD analyses using a POSS disdrometer. Part I: Precipitation cases in Busan, Journal of the Korean Meteorological Society, 40, 557-570, 2004.

Keat, W. J., Westbrook, C., Illingworth, A.: Measurements of the co-polar coefficient in rainfall and retrieval of the drop size distribution, 37th AMS on radar conference, 2015.

Mishchenko, M. I., Travis, L. D., and Mackowski, D. W.: T-matrix computations of light scattering by nonspherical particles: A review, Journal of Quantitative Spectroscopy and Radiative Transfer, 55, 535-575, 1996.

Loffler-Mang, M., Joss, J.: An optical disdrometer for measuring size and velocity of hydrometeors, J. Atmos. Oceanic. Technol., 17, 130-139, 2000

Marks, D. A., Wolff, D. B., Carey, L. D., and Tokay, A.: Quality control and calibration of the dual-polarization radar at Kwajalein, RMI. Journal of Atmospheric and Oceanic Technology, 28: 181–196, 2011.

May, P., Keenan, T. D., Zrnic, D. S., Carey, L., and Rutledge, S.: Polarimetric radar measurement of tropical rain at 5-cm wavelength, Journal of Applied Meteorology, 38, 750-765, 1999.

Ryzhkov, A. V. and Zrnic, D. S.: Discrimination between rain and snow with a polarimetric radar, Journal of Applied Meteorology, 37, 1228-1240, 1998.

Ryzhkov, A. V. and Zrnic, D. S: Assessment of rainfall measurement that uses specific differential phase, Journal of Applied Meteorology, 35, 2080-2090, 1996.

Ryzhkov, A. V., Schuur, T. J., Burgess, D. W., Heinselman, P. L., Giangrande, S. E., and Zrnic, D. S.: The Joint Polarization Experiment: Polarimetric rainfall measurements and hydrometeor classification, Bulletin of the American Meteorological Society, 86, 809-824, 2005a.

Ryzhkov, A. V., Giangrande, S. E., Melnikov, V. M., and Schuur, T. J.: Calibration issues of dual-polarization radar measurements. Journal of Atmospheric and Oceanic Technology, 22: 1138–1155, 2005b.

Ryzhkov, A., Dieberich, M., Zhang, P., and Simmer, C.: Potential utilization of specific attenuation for rainfall estimation, mitigation of partial beam blockage, and radar networking, Journal of Atmospheric and Oceanic Technology, 31, 599-619, 2014.

Sheppard, B. E.: Measurement of raindrop size distributions using a small Doppler radar, Journal of Atmospheric and Oceanic Technology, 7, 255-268.

Suk, M., Nam, K., Kim, Y., and Oh, S.: Estimation of quantitative rain intensity from radar reflectivities using a wind probability matching method, Journal of the Korean Meteorological Society, 41, 123-138, 2005.

Trabal, J. M., V. Chandrasekar, E. Gorgucci and D. J. McLaughlin, 2009: Differential reflectivity(ZDR) calibration for CASA radar network using properties of the observed medium, Geoscience and Remote Sensing Symposium,2009 IEEE International,IGARSS 2009 (Volume:2) II-960-II963.

You, C., Lee, D., Jang, M., Uyeda, H., Shinoda, T., and Kobayashi, F.,: Characteristics of rainfall systems accompanied with Changma front at Chujado in Korea, Asia-Pacific Journal of Atmospheric Sciences, 46, 41-51, 2010.

You, C., Lee, D., Jang, M., Seo, K., Kim, K., and Kim, B.: The characteristics of rain drop size distributions using a POSS in Busan area, Journal of the Korean Meteorological Society, 40, 713-724, 2004.

You, C.-H., Lee, D.-I., Kang, M.-Y.: Rainfall estimation using specific differential phase for the first operational polarimetric radar in Korea, Advances in Meteorology, vol. 2014, Article ID 41317, 10 pages, doi:10.1155/2014/413717, 2014.

You, C.-H. and Lee, D.-I.: Algorithm development of the optimum rainfall estimation using polarimetric variables in Korea. Advances in Meteorology, vol. 2015, Article ID 395937, 15 pages, doi:10.1155/2015/395937, 2015a.

You, C.-H. and Lee, D.-I.: Decadal variation in raindrop size distributions in Busan, Korea, Advances in Meteorology, vol. 2015, Article ID 329327, 8 pages, 2015, doi:10.1155/2015/329327, 2015b.

Vivekanandan, J., Zrnic, D. S., Ellis, S. M., Oye, R., Ryzhkov, A. V., and Straka, J.: Cloud microphysics retrieval using S-band dual-polarization radar measurements, Bulletin of the American Meteorological Society, 80, 381-388, 1999.

Waterman, P. C.: Symmetry, unitarity, and geometry in electromagnetic scattering, Physical Review D, 3, 825-839, 1971.

Wilson, J. W. and Brandes, E. A.: Radar measurement of rainfall-A summary, Bulletin of the American Meteorological Society, 60, 1048-1058, 1979.

Table 1. Rainfall cases used in this study.

CASE	Date and Time	Sources

Case 1	2012. 08. 23. 0900 LT ~ 1700 LT	Indirect effect of Typhoon
Case 2	2012. 09. 08. 0100 LT ~ 0600 LT	Low pressure accompanied with front
Case 3	2014. 08.25. 0900 LT ~ 1600 LT	Low pressure

Table 2. Polarimetric radar rainfall relations used in this study.

Relations		Relations	
$R(Z)$	$R=0.017Z^{0.714}$	$R(K_{DP})$	$R=61.5K_{DP}^{0.908}$
$R(A_H)$	$R=3409A_H^{1.02}$	$R(Z,Z_{DR})$	$R=0.0148Z^{0.818}Z_{DR}^{-3.72}$
$R(K_{DP},Z_{DR})$	$R=82.2K_{DP}^{0.855}Z_{DR}^{-1.977}$	$R(Z,K_{DP},A_H)$	$R=17211Z^{-0.027}K_{DP}^{0.62}A_H^{0.65}$
$R(Z,Z_{DR},K_{DP},A_H)$		$R=4502Z^{-0.14}Z_{DR}^{-0.389}K_{DP}^{0.486}A_H^{0.653}$	

Table 3. Statistics of the comparison of hourly rainfall amount between $R(Z,Z_{DR})$ and gages with different Z_H and Z_{DR} bias sources for each case.

Z_H bias source	Z_{DR} bias source	Cases	RMSE	NE	CC
Observed Z_{DR}	Observed Z_{DR}	1	5.3	0.94	0.87
		2	7.5	0.47	0.85
		3	17.2	0.66	0.77
	mZ_{DR}	1	4.9	0.67	0.87
		2	7.0	0.44	0.84
		3	9.2	0.56	0.95
mZ_{DR}	Observed Z_{DR}	1	3.9	0.67	0.87
		2	7.3	0.45	0.85
		3	15.2	0.53	0.77
	mZ_{DR}	1	3.6	0.63	0.89
		2	6.8	0.43	0.84
		3	7.4	0.45	0.95

Table 4. Same as Table 3 but for $R(Z,Z_{DR},K_{DP},A_H)$.

Z_H bias source	Z_{DR} bias source	Cases	RMSE	NE	CC
Observed Z_{DR}	Observed Z_{DR}	1	3.2	0.53	0.74
		2	6.6	0.4	0.86
		3	5.2	0.3	0.95
	mZ_{DR}	1	3.2	0.53	0.74
		2	6.7	0.4	0.86
		3	5.2	0.3	0.95
mZ_{DR}	Observed Z_{DR}	1	3.1	0.52	0.74
		2	6.7	0.4	0.86
		3	5.3	0.3	0.95
	mZ_{DR}	1	3.1	0.52	0.74
		2	6.7	0.4	0.86
		3	5.4	0.31	0.95

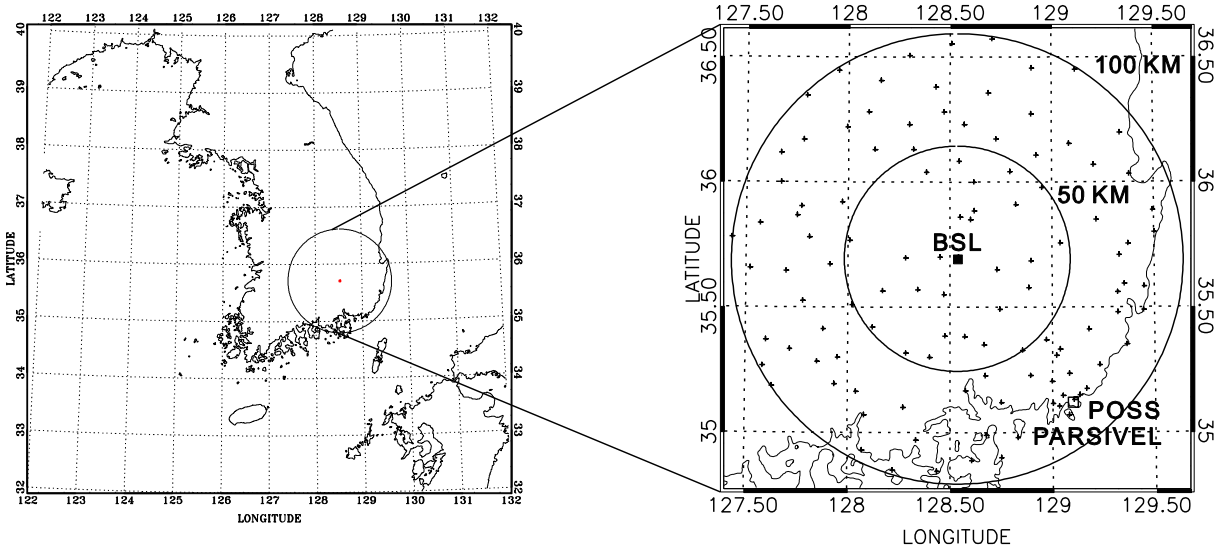

Figure 1. Location of Bislsan radar (solid rectangle), the POSS and PARSIVEL disdrometer (open rectangle), and rain gages (plus signs) distributed within 100 km of the radar. The circles are at 50 and 100 km from the radar.

(a)

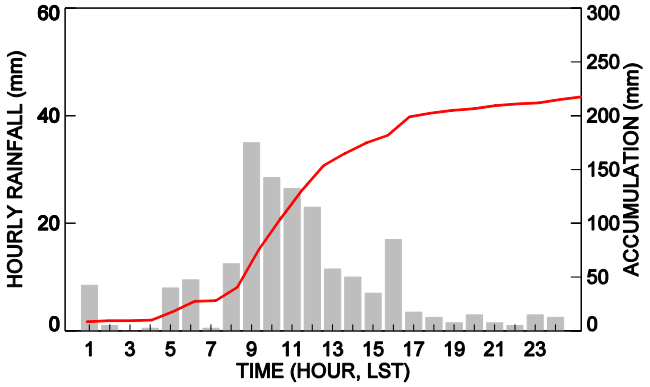

(b)

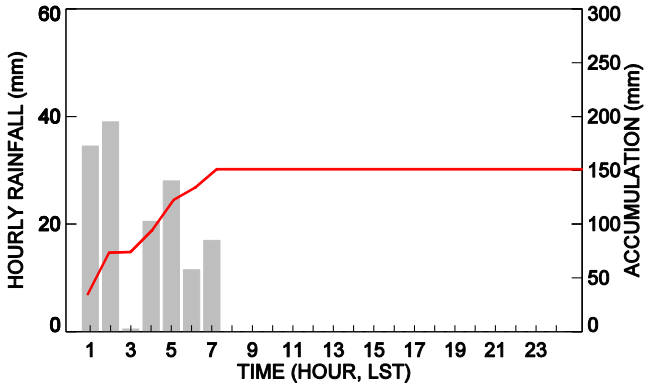

(c)

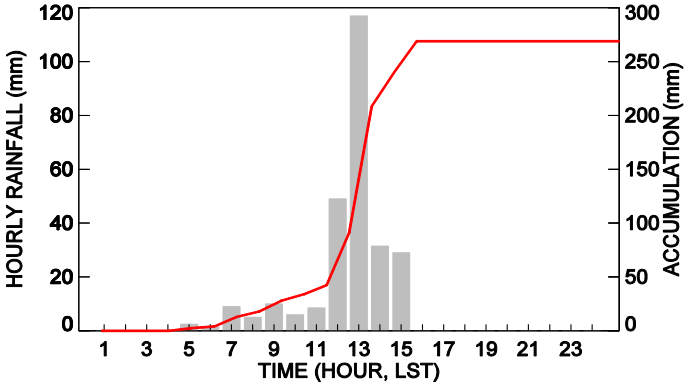

Figure 2. Time series of hourly rainfall (gray bars) and accumulation (red line) from the three gages that recorded the highest rainfall (a) 23 August 2012 at ID 945, (b) 8 September 2012 at ID 255, and (c) 25 August 2014 at ID 926.

(a)

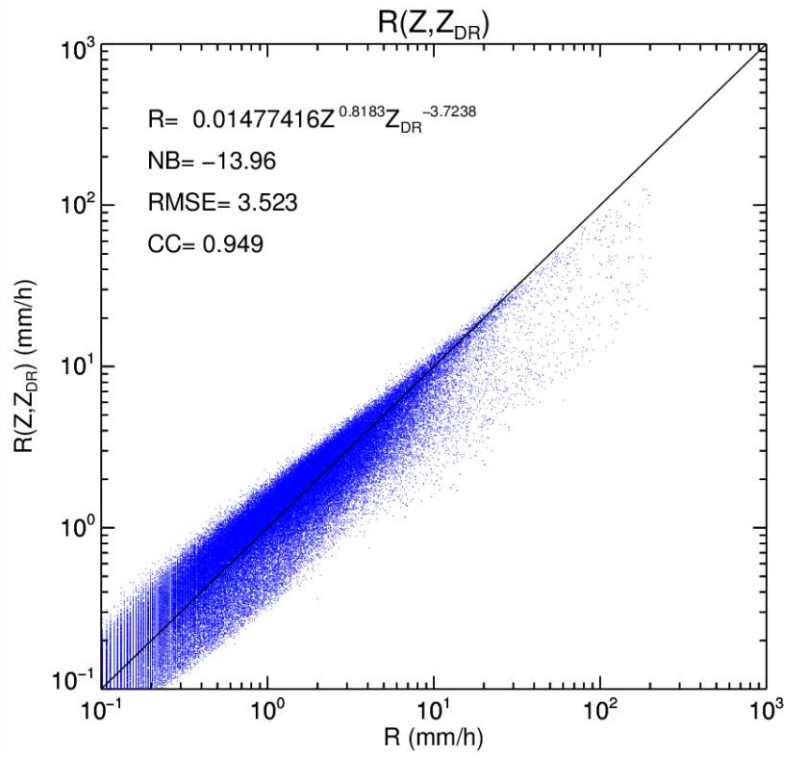

(b)

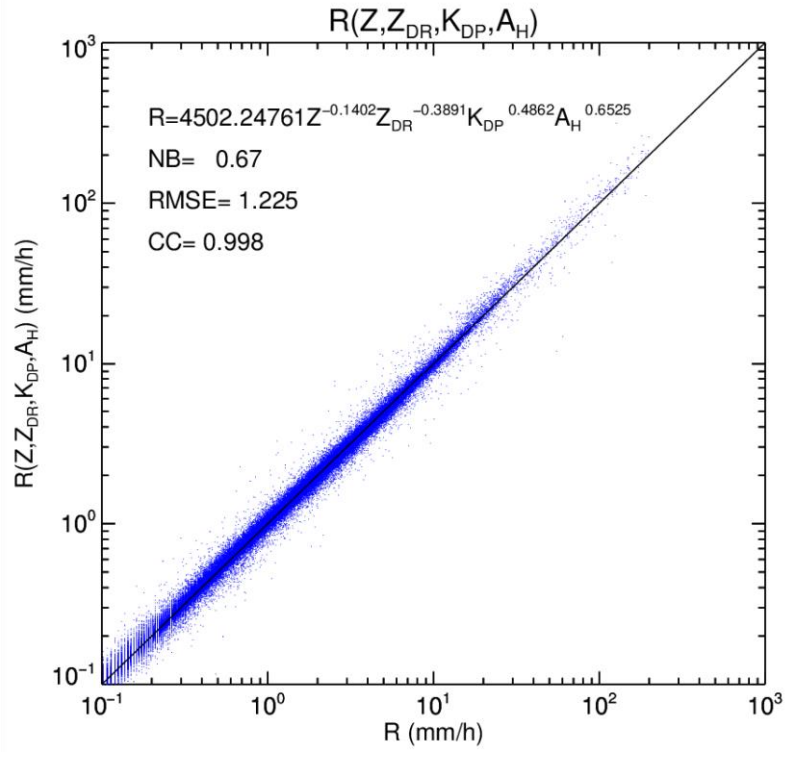

Figure 3. Scatter plot of rain rate measured by disdrometer and polarimetric radar rainfall relation (a) R(Z,ZDR) and R(Z,ZDR,KDP,AH). The rainfall relation and statistical values are also shown.

(a)

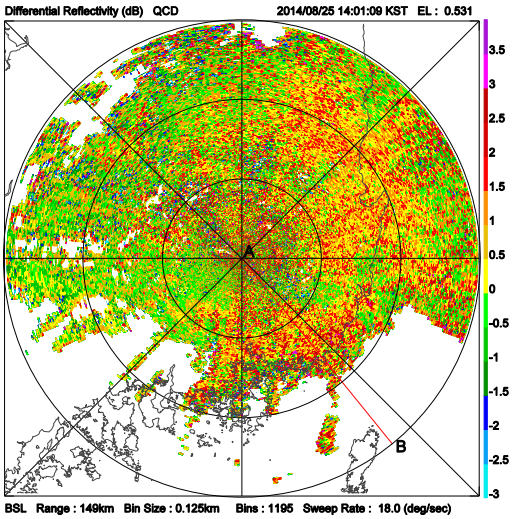

(b) (c)

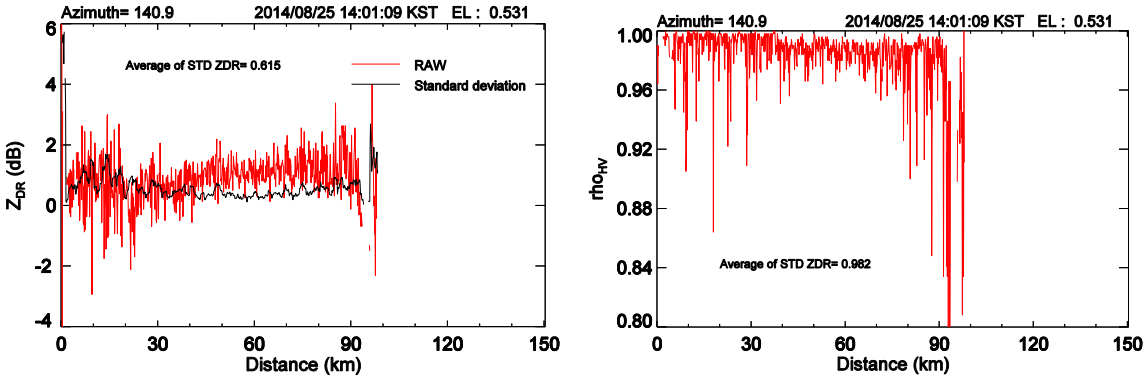

Figure 4. (a) Distribution of Z_{DR} within the radar coverage, (b) the radial profile of Z_{DR} and (c) cross correlation along the line A–B in (a) at 1401 LT 25 August 2014.

(a) (b)

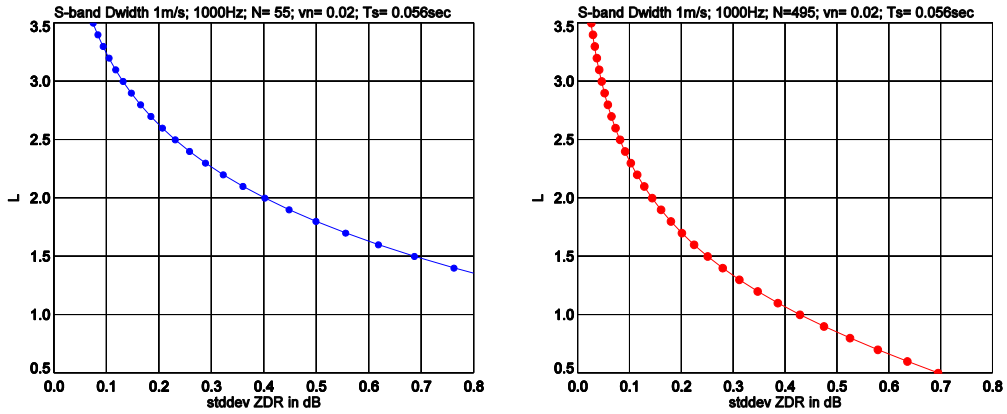

Figure 5. Theoretical relation between standard deviation of Z_{DR} and cross correlation using (a) the scan configuration of the Bislsan radar. Dwell time is 56 ms, number of samples is 55, normalized Doppler width is 0.02; (b) same as (a) but for 495 samples.

(a)

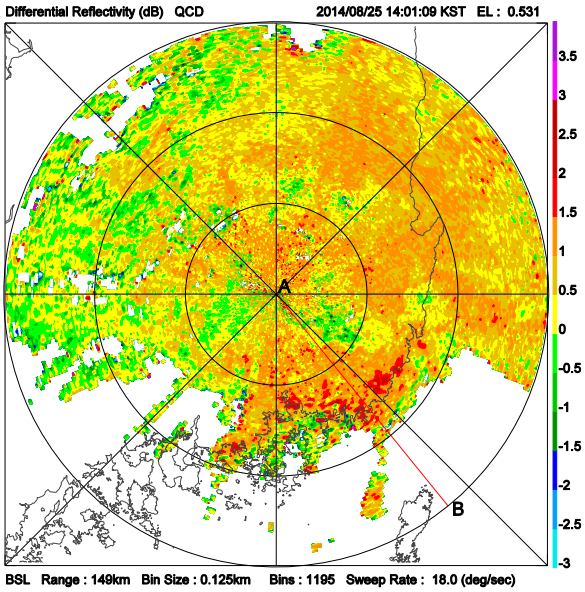

(b) (c)

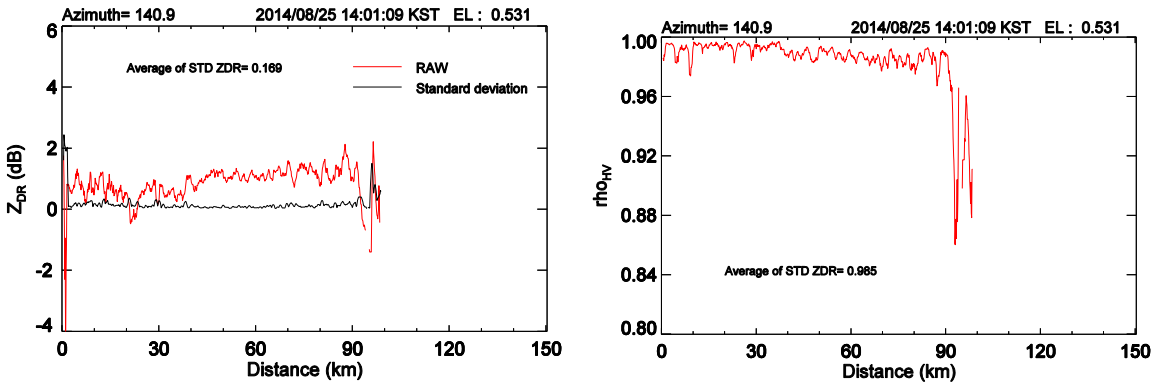

Figure 6. Same as Fig. 4 but for moving averages of Z_{DR}.

(a)

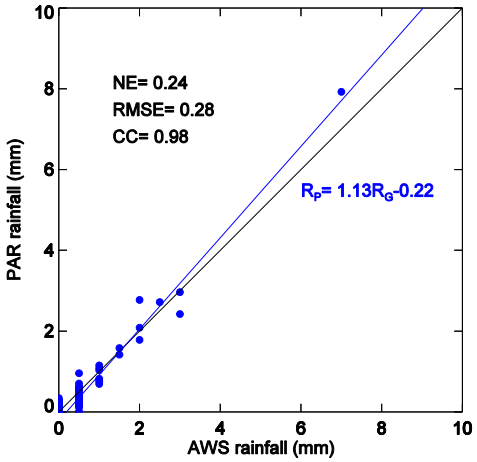

(b)

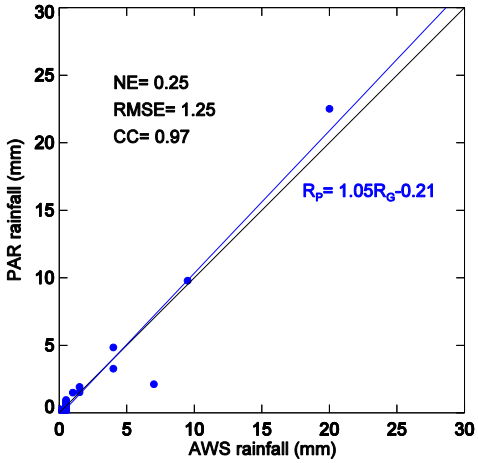

(c)

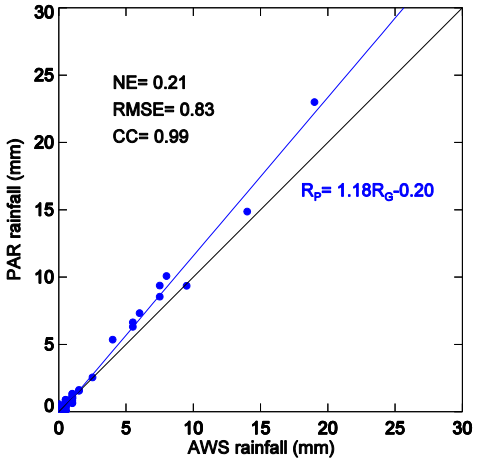

Figure 7. Scatter plot of 10 min rainfall amount measured by PARSIVEL and gage for 24 hours for (a) Case 1, (b) Case 2, and (c) Case 3, respectively.

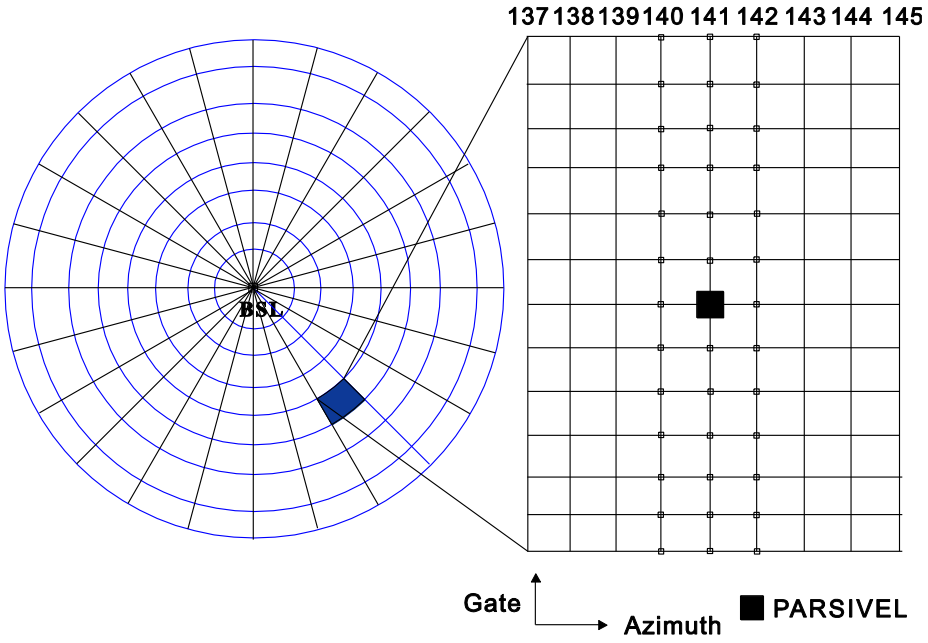

Figure 8. Schematic diagram for the comparison of radar and PARSIVEL Z_{DR}. The numbers refer to azimuth angle.

(a) (b)

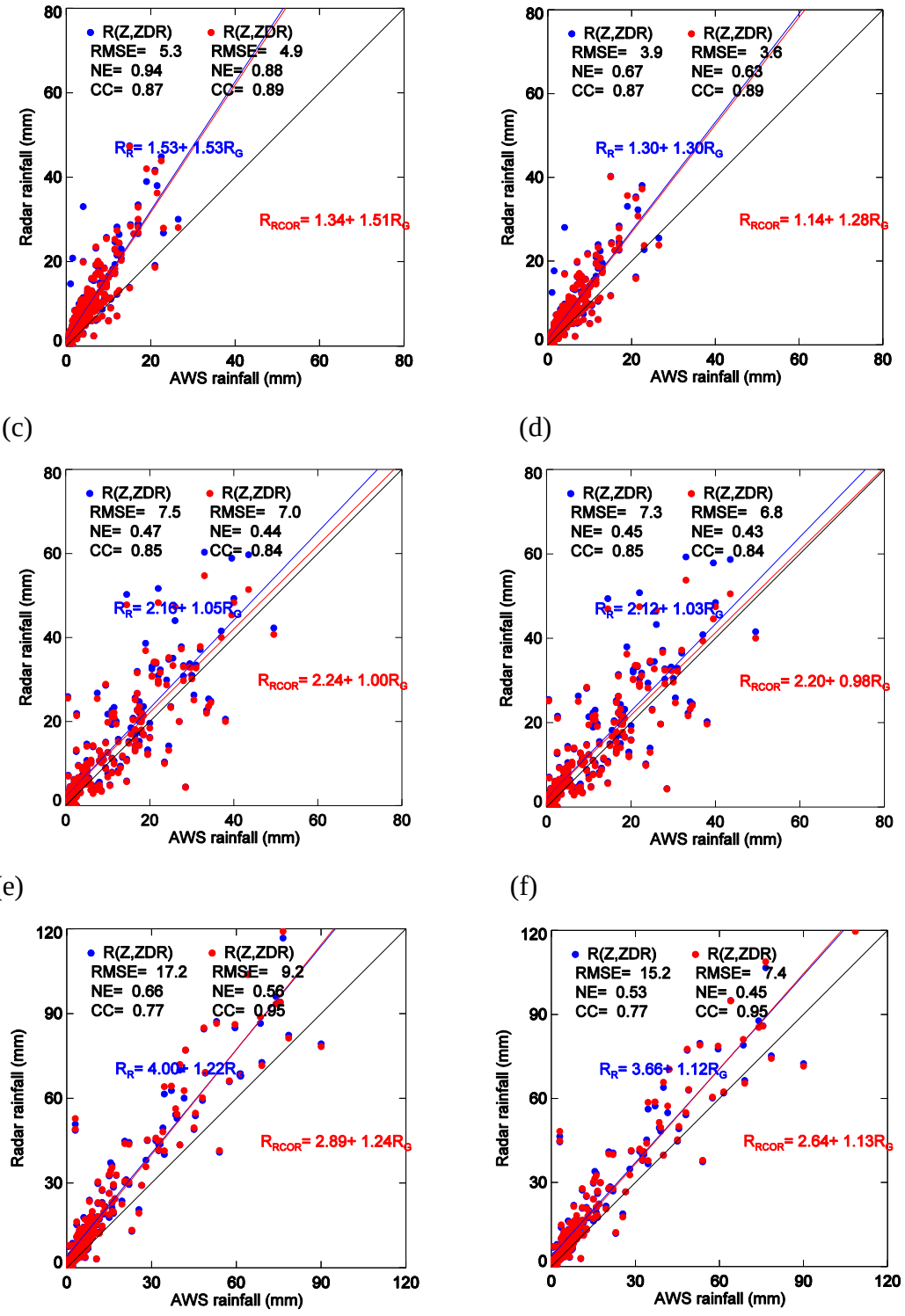

Figure 9. Scatter plot of 1 hour rainfall obtained by R(Z,Z_{DR}) against gage rainfall. (a, c, e) Radar rainfall was calculated using Z_H bias calculated from observed Z_{DR} bias and Z_{DR} biases calculated from observed Z_{DR} (blue full circles) and mZ_{DR} (red full circles), (b, d, f) same as (a, c, e) but for Z_H bias calculated from mZ_{DR} on Case 1, Case 2, and Case 3, respectively.

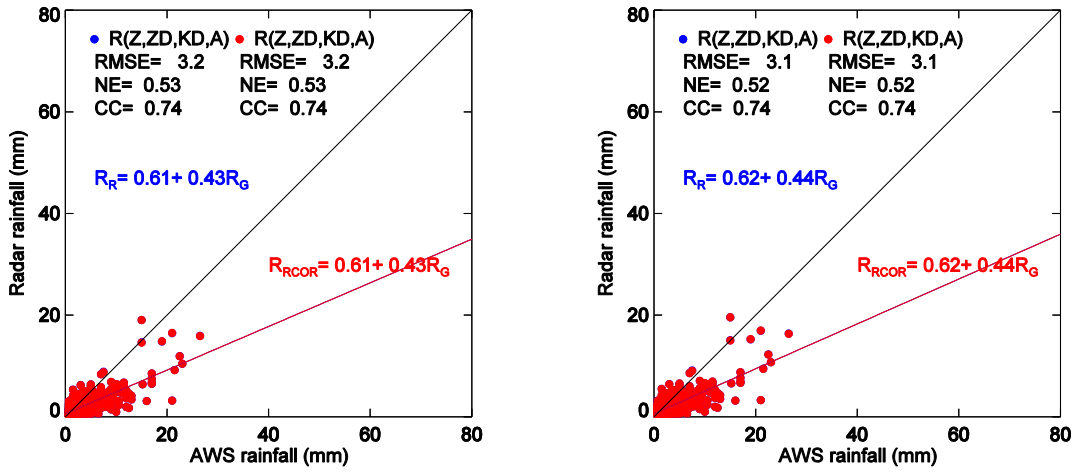

(c) (d)

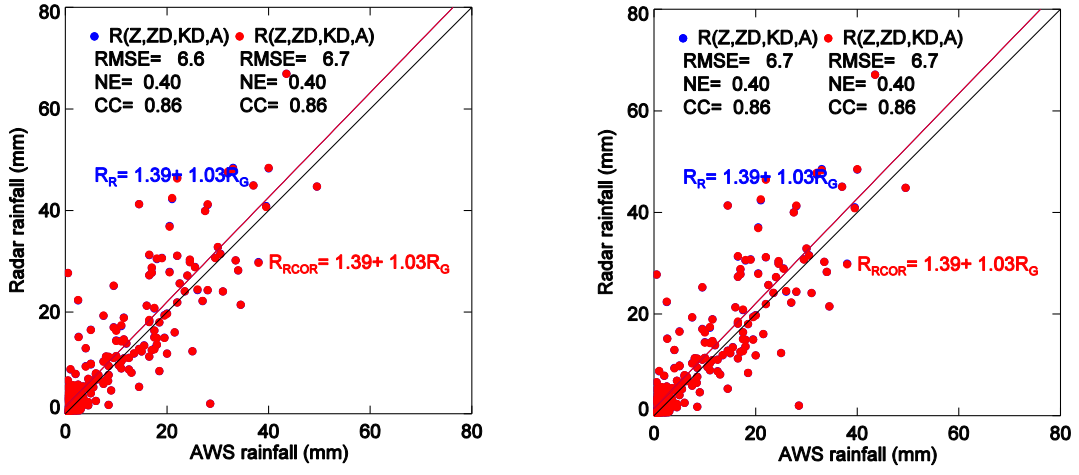

(e) (f)

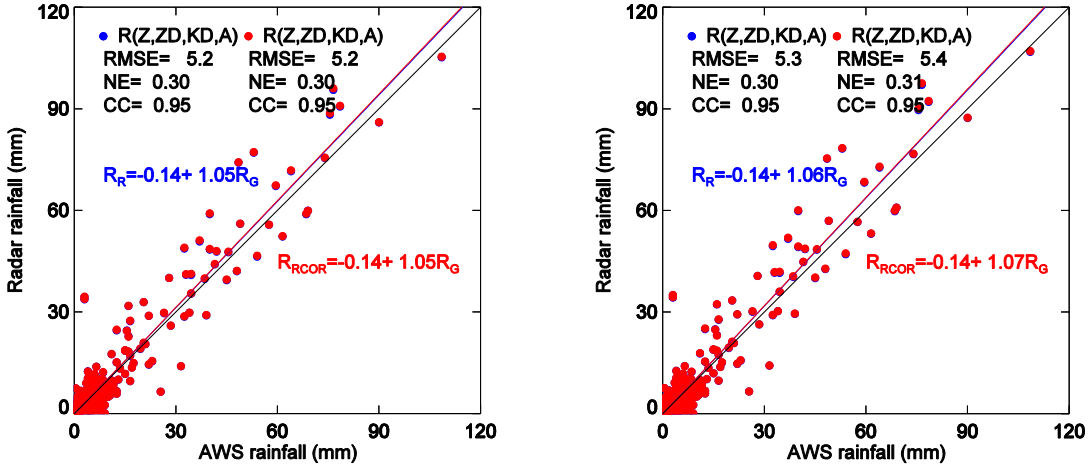

Figure 10. Same as Fig. 9 but for radar rainfall obtained by $R(Z,Z_{DR},K_{DP},A_H)$.

(a) (b)

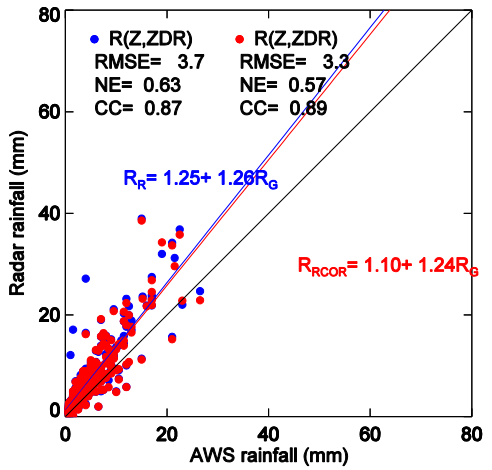

(c)

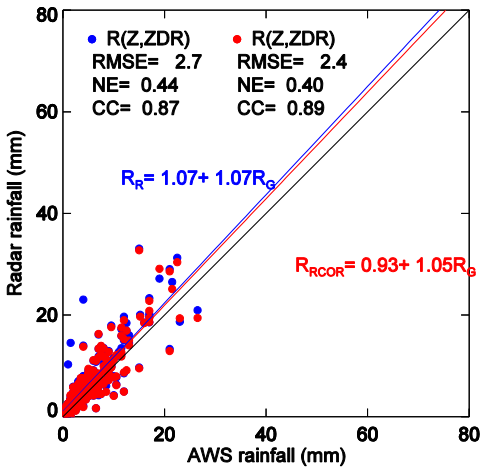

(d)

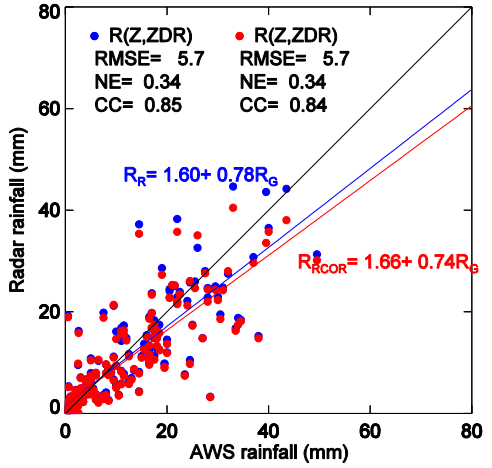

(e)

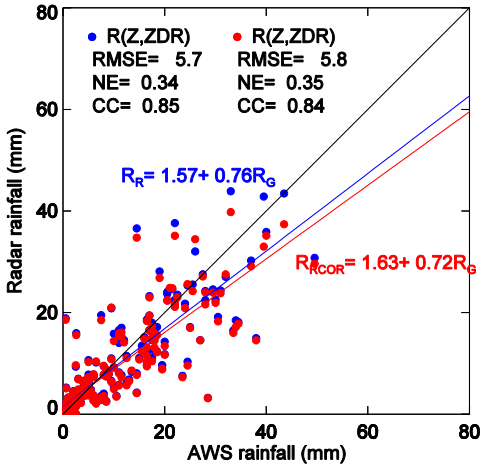

(f)

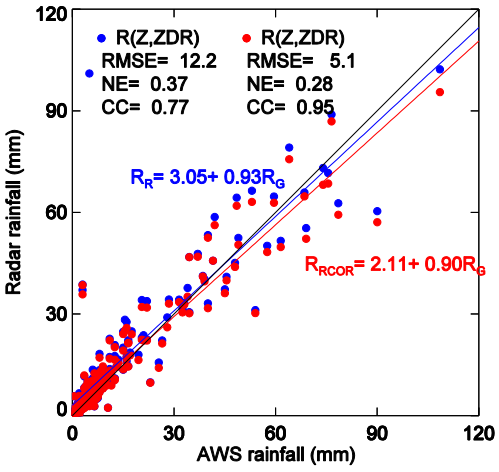

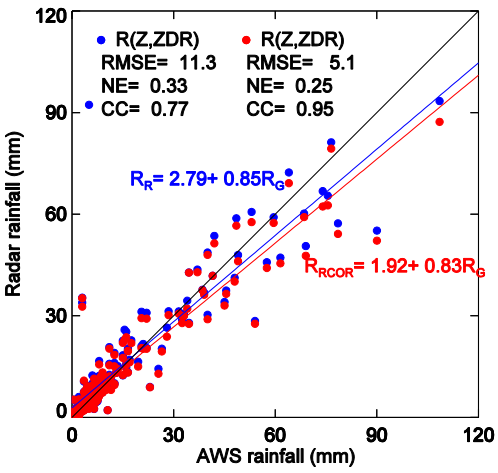

Figure 11. Same as Fig. 7 but for Z_{DR} biases determined by PARSIVEL.

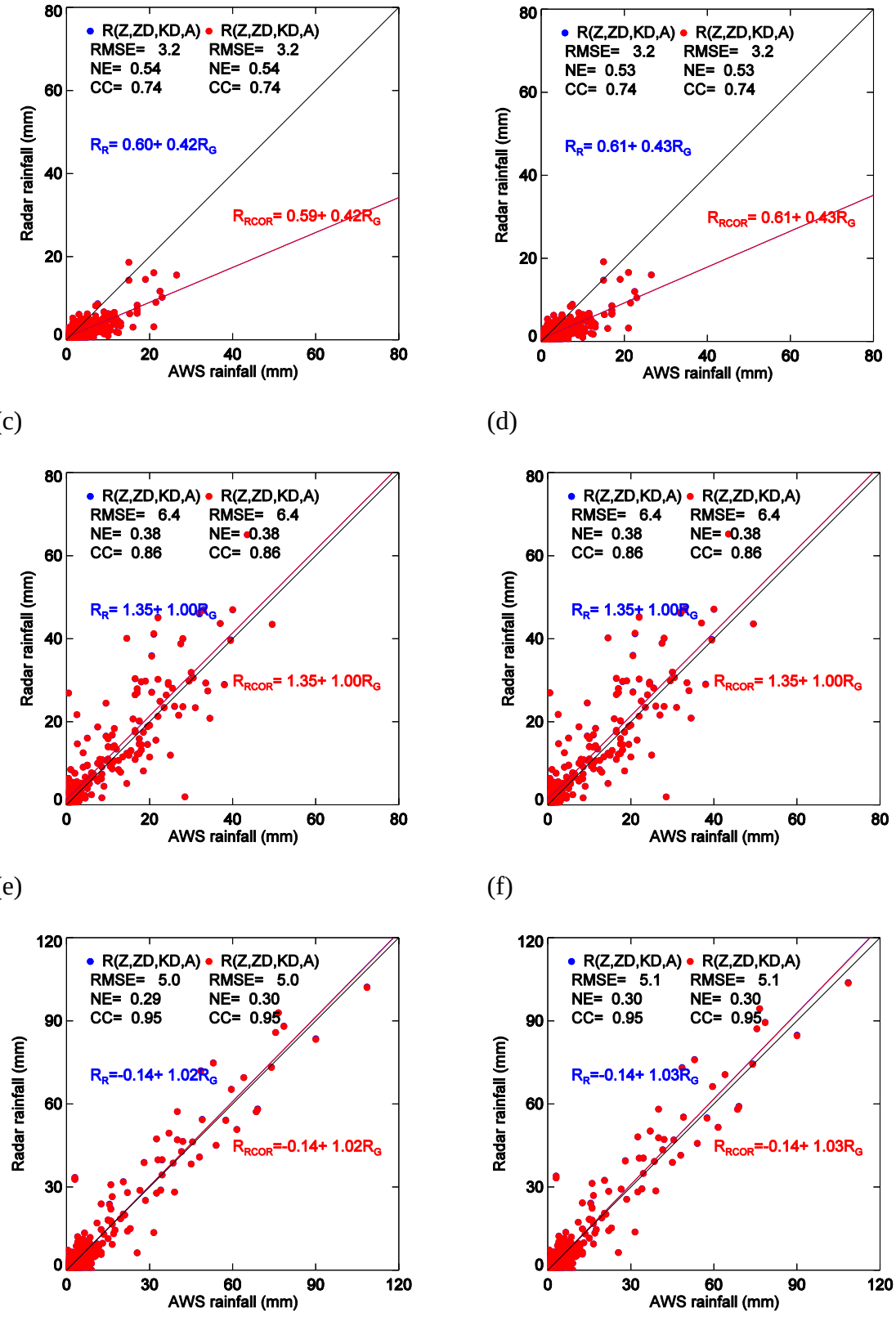

Figure 12. Same as Fig. 8 but for Z_{DR} biases determined by PARSIVEL.

(a) (b)

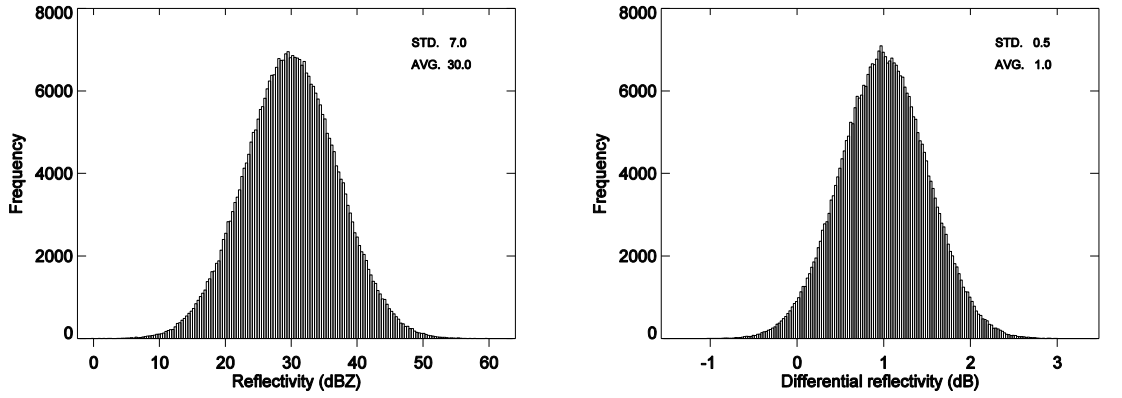

(c) (d)

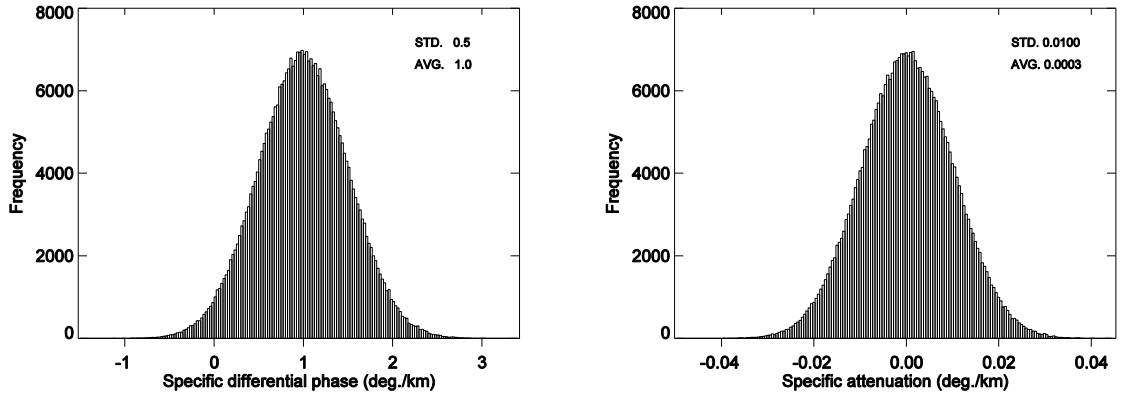

Figure 13. Distribution frequencies of the generated polarimetric variables. (a) Z_H, (b) Z_{DR}, (c) K_{DP}, and (d) A_H.

(a)

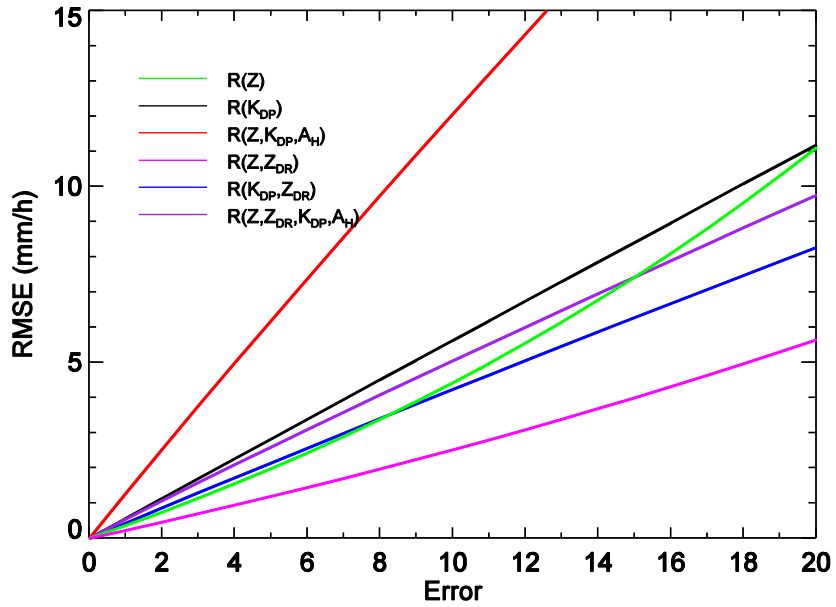

(b)

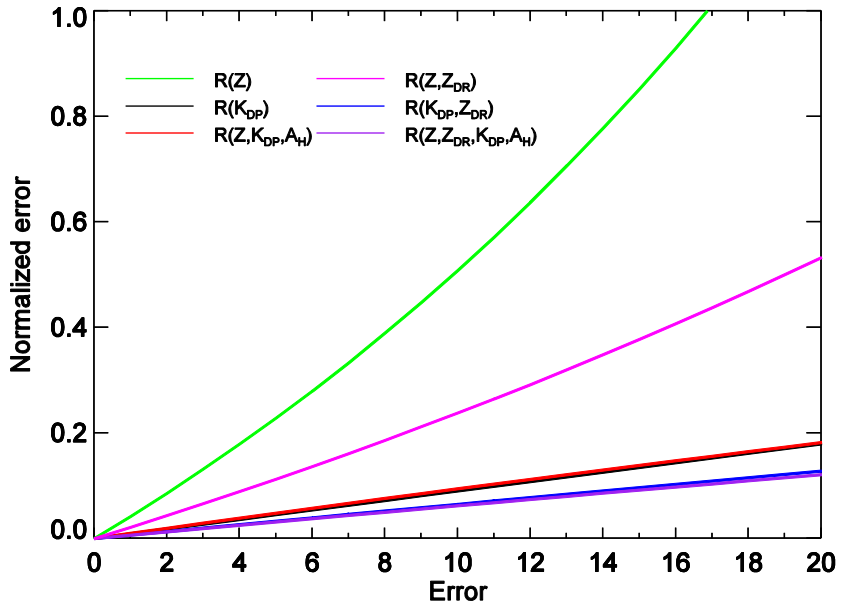

Figure 14. Distribution of (a) RMSE and (b) NE with generated errors for different rainfall relations. Magenta, black, red, green, blue, and purple lines show RMSE and NE obtained from the rainfall relations R(Z), R(K_{DP}), R(Z,K_{DP},A_H), R(Z,Z_{DR}), R(K_{DP},Z_{DR}), and R(Z,Z_{DR},K_{DP},A_H), respectively.